Twenty-Seventh Symposium (International) on Combustion/The Combustion Institute, 1998/pp. 615–623

EXPERIMENTAL AND COMPUTATIONAL STUDY OF CH, CH*, AND OH* IN AN AXISYMMETRIC LAMINAR DIFFUSION FLAME

K. T. WALSH, M. B. LONG, M. A. TANOFF AND M. D. SMOOKE
Department of Mechanical Engineering
Yale University
New Haven, CT 06520-8284, USA

In this study, we extend the results of previous combined numerical and experimental investigations of an axisymmetric laminar diffusion flame in which difference Raman spectroscopy, laser-induced fluorescence (LIF), and a multidimensional flame model were used to generate profiles of the temperature and major and minor species. A procedure is outlined by which the number densities of ground-state CH ($X^2\Pi$), excited-state CH ($A^2\Delta$, denoted CH*), and excited-state OH ($A^2\Sigma$, denoted OH*) are measured and modeled. CH* and OH* number densities are deconvoluted from line-of-sight flame-emission measurements. Ground-state CH is measured using linear LIF. The computations are done with GRI Mech 2.11 as well as an alternate hydrocarbon mechanism. In both cases, additional reactions for the production and consumption of CH* and OH* are added from recent kinetic studies. Collisional quenching and spontaneous emission are responsible for the de-excitation of the excited-state radicals.

As with our previous investigations, GRI Mech 2.11 continues to produce very good agreement with the overall flame length observed in the experiments, while significantly under predicting the flame lift-off height. The alternate kinetic scheme is much more accurate in predicting lift-off height but overpredicts the overall flame length. Ground-state CH profiles predicted with GRI Mech 2.11 are in excellent agreement with the corresponding measurements, regarding both spatial distribution and absolute concentration (measured at 4 ppm) of the CH radical. Calculations of the excited-state species show reasonable agreement with the measurements as far as spatial distribution and overall characteristics are concerned. For OH*, the measured peak mole fraction, 1.3×10^{-8}, compared well with computed peaks, while the measured peak level for CH*, 2×10^{-9}, was severely underpredicted by both kinetic schemes, indicating that the formation and destruction kinetics associated with excited-state species in flames require further research.

Introduction

CH has long been recognized as a key reactant in NO_x formation through the prompt NO mechanism. Given that CH is a short-lived trace species that exists in a narrow spatial and temperature region within a flame, its concentration and spatial distribution are very sensitive tests of the detailed chemical kinetics needed to model pollutant formation. The oxidation of CH plays a central role in the production of chemically excited OH ($A^2\Sigma$, denoted OH*), which emits in the ultraviolet. This ultraviolet emission has been suggested as a measure of the final steps of the CH_x reduction chain [1]. Chemically excited CH ($A^2\Delta$, denoted CH*) is responsible for the blue light in low-soot flames and may provide insight into the C_2 reaction chain [1]. Despite the prevalence of CH* and OH* chemiluminescence, little quantitative work has been done either experimentally or computationally in predicting the absolute concentrations of these species. In this study, quantitative measurements of CH, CH*, and OH* are performed and comparisons are made with computational predictions.

The flame under investigation is a lifted axisymmetric laminar diffusion flame, which has been characterized previously both experimentally and computationally [2–5]. The fuel is nitrogen-diluted methane surrounded by an air coflow. Experimentally, temperature and major species (CH_4, N_2, O_2, H_2O, CO, CO_2, H_2) concentrations were measured simultaneously with Rayleigh and Raman scattering [2]. Laser-induced fluorescence (LIF) measurements were performed to measure number densities of minor species. Quantitative, linear LIF measurements were made for OH [3] and NO [4], and qualitative measurements of CH have been made [3]. Modeling work has employed different kinetics schemes, including a 26-species C_2 hydrocarbon mechanism [3] and GRI Mech 2.11. Both produced excellent agreement for temperature and major species [5]. Computed peak concentrations for NO and OH were within 30% and 15%, respectively, of their measured values.

In the following sections, the experimental configuration is described, and the details of the measurements of CH, CH*, and OH* are presented. The

computational model and the various kinetics schemes used to predict the measured species are then described. Finally, the experimental results are compared with computations based on different kinetics schemes.

Burner Configuration

The burner used in this experiment consisted of a central fuel jet (4 mm diameter) surrounded by coflowing air (50 mm diameter). The fuel was composed of 65% methane diluted with 35% nitrogen by volume to reduce soot, and the plug flow exit velocity of both fuel and coflow was 35 cm/s. This produces a blue flame roughly 3 cm in length with a lift-off height of 5.5 mm. Complete burner specifications are given elsewhere [2]. The burner was mounted on a stepper motor to allow measurements to be taken at different heights.

Laser-Induced Fluorescence Measurement of CH

The third harmonic of a Nd:YAG laser, operating at 10 Hz, pumped a dye laser containing Coumarin 440 dye. The R(7) line in the (0,0) band of the *A–X* system, near 426.8 nm, was selected for excitation. The dye beam was split for power measurement, attenuated, shaped into a sheet, and passed across the jet centerline. Typical energies were 1 μJ per pulse. The laser sheet dimensions were measured to be 5.5 mm $\times$ 300 μm. The measured line width $\Delta\nu$ of the beam was 0.16 cm^{-1}, and the pulse duration was 10 ns, which corresponds to a spectral density of order 10^4 W/(cm^2 cm^{-1}), well below the saturation value [6]. Imaging was done with a cooled charged-coupled device (CCD) camera and a lens-coupled image intensifier. The CH fluorescence was isolated with an interference filter that transmitted from 400 to 440 nm. An f/2 camera lens collected the CH fluorescence, and a pair of f/1.4 camera lenses focused the light from the back end of the intensifier onto the CCD chip. The imaged pixel volume was 30 $\times$ 30 $\times$ 300 μm^3. The laser was set to 426.777 nm to record on-resonance images (I_{on}) and to 426.671 nm for off-resonance images (I_{off}). A flame luminosity image was also taken with the laser turned off (I_{lum}). Typical images were integrated over 6000 laser shots. The on-resonance image contained LIF and Rayleigh scattering on top of the flame luminosity background, while the off-resonance image had only Rayleigh scattering and flame luminosity. Because the laser energy differed by a small known amount between the on- and off-resonance measurements (E_{on} and E_{off}), the final LIF images were created as follows: $S_{LIF} = I_{on} - I_{lum} - (I_{off} - I_{lum})^* E_{on}/E_{off}$. Measurements were made at each of eight heights above the burner surface, and these images were later tiled together.

To convert the measured LIF signal into a quantitative concentration measurement, a number of calibrations and corrections must be made. For a two-level model, the LIF signal per pulse in the linear regime is given by

$$S_{LIF} = \frac{1}{4\pi} b_{12} \frac{E_{LIF}}{A_{LIF}\Delta\nu} n_{CH} f_B \Gamma \times \underbrace{\frac{A_{21}}{A_{21} + Q_{21}}}_{\Phi} V_{LIF} \Omega \varepsilon \eta \qquad (1)$$

where b_{12} is the absorption rate, E_{LIF} is the laser energy per pulse, $\Delta\nu$ is the laser line width, A_{LIF} is the cross-sectional area of the laser beam, n_{CH} is the number density of ground-state CH, f_B is the fraction of the ground state in the state being pumped, Γ is a dimensionless overlap integral, A_{21} is the spontaneous emission rate, Q_{21} is the collisional quenching rate, V_{LIF} is the LIF pixel volume, Ω is the solid angle over which light is collected, ε is the efficiency of the collection optics, and η is the detector efficiency in counts per photon [7]. The quantity that we are interested in determining is n_{CH}. The factors in equation 1 must be measured directly or determined from the literature. The quantity $A_{21}/(A_{21} + Q_{21})$ represents the fraction of excited molecules that emit a photon and is called the fluorescence yield, Φ. The total collisional quenching rate for the excited state is $Q_{21} = \Sigma c_i k_i$, where c_i is the concentration of species i and k_i is the collisional quenching rate for species i. Values for k_i (which are temperature dependent) were computed from the functional form given by Tamura et al. [8]. Concentration profiles of the major species (CH_4, N_2, O_2, H_2O, CO, CO_2, H_2) were computed previously [5] and used for these calculations. The temperature in the thin region where CH is present is nearly constant at 1900 K. This quenching calculation resulted in a spatially constant fluorescence yield Φ of 1/176. In this flame, N_2 was responsible for more than 60% of the quenching. Unfortunately, the CH/N_2 quenching rate has not been measured above 1300 K making the extrapolation to flame temperatures a source of uncertainty. The Boltzmann factor, f_B, is calculated based on the molecule probed, temperature, and the excitation/detection scheme used. Given our choice of the R(7) line, $f_B = 0.07$. Spectroscopic rotational and vibrational constants were taken from Huber and Herzberg [9]. Γ is a spectral integral of the overlap between the CH absorption profile and the laser beam. The laser profile was fit to a Gaussian distribution centered at 426.777 nm with a full width at half-maximum (FWHM) of $\Delta\nu = 0.16$ cm^{-1}, measured previously. The absorption spectrum of CH (at

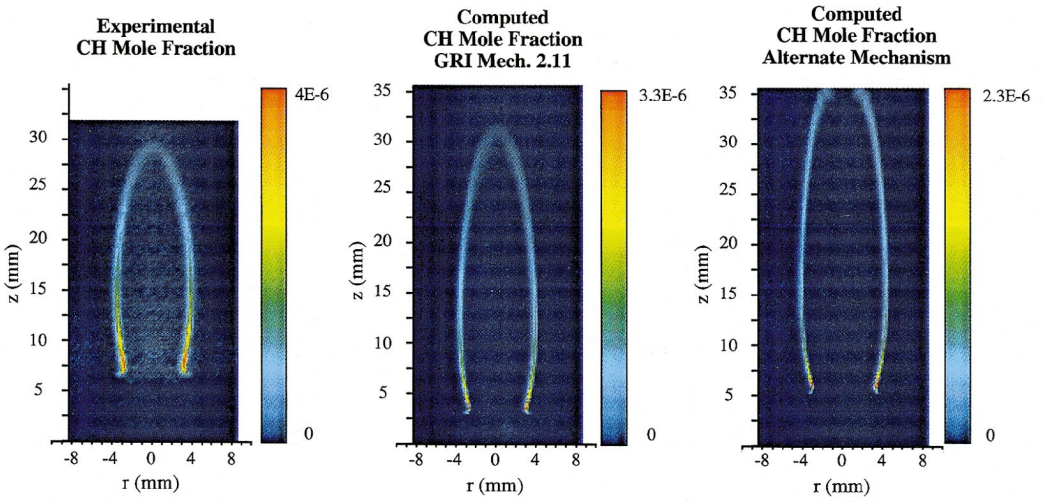

FIG. 1. CH mole fraction profiles determined by measurement, GRI Mech 2.11, and an alternate hydrocarbon mechanism.

atmospheric pressure with resolution $\Delta\nu$) was calculated with the LIFBASE program [10] and resulted in $\Gamma = 0.17$. The calculated absorption profile was needed because a CH excitation spectrum could not be measured practically in the linear regime given the long integration times needed to obtain reasonable signal levels. A saturated CH excitation scan was performed, however, and compared well to a computed absorption profile for a larger line width. When evaluating the integral, both the computed absorption profile (with line width $\Delta\nu$) and fit beam profile had narrow features. Small variations in the peak of the Gaussian, hence small changes in the laser wavelength, affect Γ. Given that the resettability of the dye laser is ± 0.02 Å, the uncertainty in Γ is estimated at 20%.

Rayleigh Calibration

Calibration of CH LIF is somewhat problematic. CH is highly reactive, preventing reference to a known concentration, and is present in a very thin (~500 μm wide) region, making absorption calibration difficult. However, Luque and Crosley [7] have demonstrated that Rayleigh scattering can be used on the same optical setup to relate the measured signal to an absolute light level and thus solve for the overall calibration product ($\Omega\varepsilon\eta$) in equation 1.

For scattering from a homogeneous gas, the Rayleigh signal per pulse is given by

$$S_R = \frac{NE_R V_R \left(\frac{\partial\sigma}{\partial\Omega}\right)}{A_R h\nu}\,\Omega\varepsilon\eta \qquad (2)$$

where N is the number density of the gas flow used for calibration, E_R is the laser energy per pulse producing the Rayleigh signal, V_R is the Rayleigh volume, $(\partial\sigma/\partial\Omega)$ is the Rayleigh cross section, $h\nu$ is the photon energy, and A_R is the cross-sectional area of the laser beam. After Rayleigh measurements are made, the calibration product can be eliminated, resulting in a single expression for number density. Given that the fluorescence beam occupies the same spatial region as the Rayleigh beam ($A_R = A_{LIF}$ and $V_R = V_{LIF}$), we now have

$$n_{CH} = \frac{4\pi S_{LIF}\Delta\nu N E_R \left(\frac{\partial\sigma}{\partial\Omega}\right)}{b_{12}E_{LIF}\Gamma f_B \Phi h\nu S_R} \qquad (3)$$

as an expression for absolute number density of ground-state CH.

Rayleigh calibration was done on a flow of clean air with the same optical setup and beam dimensions as used in LIF. Although calibration can be done with a single Rayleigh image, measurements were made over a range of energies to verify the linear relationship between the signal and laser energy and to confirm a zero intercept. The measured calibration was linear and had an intercept within a few percent of the origin. Energy per pulse was varied between 0.1 and 1.2 mJ, with an integration of 300 to 1500 shots.

These calibrations and calculations, in conjunction with previous temperature measurements, resulted in a two-dimensional profile of CH mole fraction that can be seen in Fig. 1. The measured peak mole fraction was 4 ppm.

Chemiluminescence of CH* and OH*

Measurements of chemically excited flame radicals, such as CH* and OH*, are relatively easy to make but have calibration difficulties similar to those of ground-state CH. Fortunately, the same Rayleigh calibrations can be applied to determine absolute intensity levels, and quenching corrections can be made to quantify the measured signals. The space and power constraints imposed by microgravity experiments have generated a renewed interest in making such emission measurements as quantitative as possible. Although flame emissions were examined spectrally decades ago and CH* has been recognized as the primary source of the ubiquitous "blue light" in low-soot flames [11], the reactions that produce CH* are not well understood. Chemiluminescent OH (OH*) is another common flame emitter whose kinetics deserve investigation. A goal of this study was to measure the absolute number densities of these flame radicals to assess the current state of CH* and OH* kinetics.

OH* chemiluminescence peaks at 307.8 nm. Excited-state OH measurements were made with a cooled CCD camera using an f/4.5 UV camera lens; the camera/lens system was placed 50 cm away to ensure a wide depth of field. A narrow bandpass UV filter was used (center 307 nm, 10 nm bandwidth). High emission signal levels were collected with 10 s integration times. Rayleigh calibration was done with a Nd:YAG-pumped dye laser utilizing sulfarhodamine 640 dye. The 612 nm output was frequency doubled to perform calibration measurements on clean air. Beam energy in the UV was varied from 0.3 to 2.0 mJ per pulse and integration times were 600 shots.

For CH* flame emission, the $A^2\Delta \rightarrow X^2\Pi$ transition at 431.2 nm was imaged with the camera and lens system detailed above. An interference filter (center 431 nm, 10 nm bandwidth) was used to isolate the CH* emission. Again, good signal levels were collected over 10 s integration times. The calibration measurements were again performed with a Nd:YAG-pumped dye laser. During Rayleigh calibration, the energy of the 431.5-nm beam was varied between 0.5 and 2.5 mJ, with signal collected over 600 shots.

The flame emission signal, in detector counts, is given by

$$S_{\mathrm{em}} = \frac{1}{4\pi} A_{21}\tau V_{\mathrm{em}} N_{\mathrm{em}} \Omega\varepsilon\eta \qquad (4)$$

where τ is the integration time, V_{em} is the pixel volume of the emission signal, and N_{em} is the number of molecules that emit a photon. The spontaneous emission rate and integration time are known, and the emission volume can be determined directly. As with the fluorescence measurement, the calibration constants of the optical system, $\Omega\varepsilon\eta$, are accounted for with Rayleigh scattering. Furthermore, a quenching calculation is needed to relate the number density of emitting molecules to the total population of the chemically excited radical. To obtain an absolute number density of a chemically excited radical, N^*, we recognize that $N^* = N_{\mathrm{em}}/\Phi$. Equations (2) and (4) can be combined with this to yield

$$N^* = \frac{4\pi S_{\mathrm{em}} N E_{\mathrm{R}} \left(\frac{\partial\sigma}{\partial\Omega}\right)\ell}{S_{\mathrm{R}} A_{21}\tau V_{\mathrm{em}}\Phi h\nu} \qquad (5)$$

where ℓ is the length along the beam in the Rayleigh volume under consideration.

Emission measurements are integrated through the collection optics along the line of sight. Appropriate background images, taken for both CH* and OH* with the flame extinguished, are subtracted from the raw emission signal. Given that our flame is axisymmetric and that the imaging optics are configured so that the magnification changes by only 1% over the flame width, we can recover a two-dimensional, in-plane intensity distribution proportional to number density with the use of an algorithm that is equivalent to a two-point Abel deconvolution [12]. After inversion, pixel volumes were determined to be cubes of side length 68 μm for both CH* and OH*. The quenching correction for CH* was performed using the cross sections and temperature determined for ground-state CH. This resulted in a peak CH* mole fraction of 2×10^{-9}, as seen in Fig. 2. For OH*, quenching rates for OH were taken from Tamura et al. [8] and combined with major species and temperature computations performed previously [5]. OH* appears at a nearly constant temperature of 1900 K and is highly localized. The quenching calculation resulted in a fluorescence yield Φ of 1/327 that did not vary spatially. Water, the only important individual collider, is responsible for about 2/3 of the OH* quenching in this flame. Cross sections for OH have been measured over a large range of temperatures and have agreed with low-pressure quenching measurements to within 5% [8]. The measured OH* profile is displayed in Fig. 3; the peak mole fraction was 1.3×10^{-8}.

Computational Model

The computational model used to compute the temperature field, velocities, and species concentrations solves the full set of elliptic two-dimensional governing equations for mass, momentum, species, and energy conservation on a two-dimensional mesh [13]. The resulting nonlinear equations are then solved on an IBM RS/6000 Model 590 computer by a combination of time integration and Newton's method. The chemical mechanisms employed were GRI Mech 2.11 [14] and an alternate hydrocarbon mechanism (used, for example, in Ref. [3]).

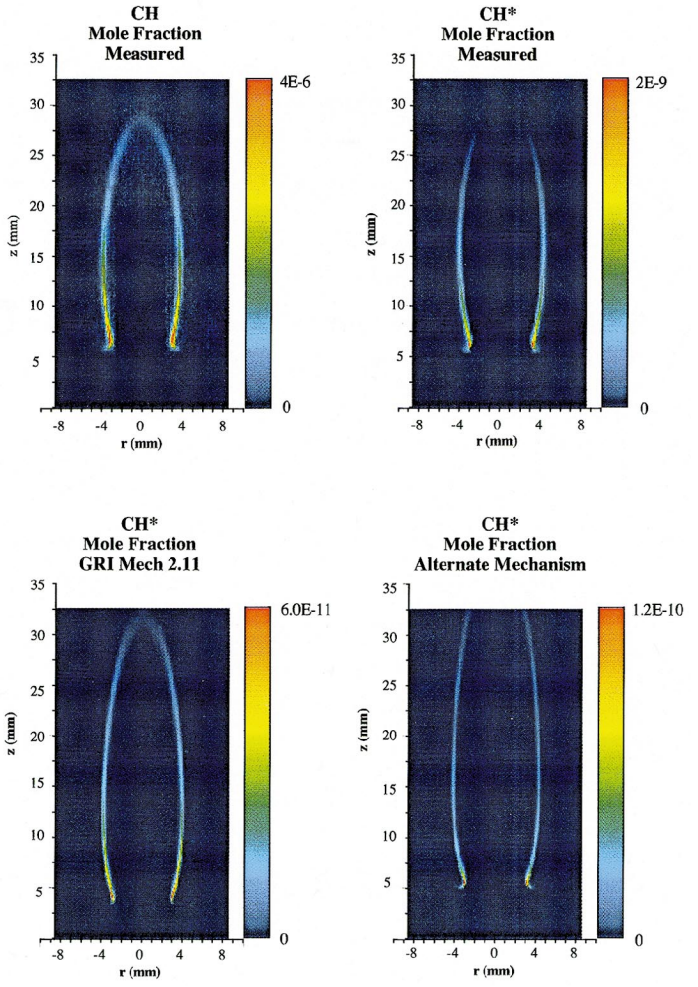

FIG. 2. CH* mole fraction profiles determined by measurement, GRI Mech 2.11, and an alternate hydrocarbon mechanism. The ground-state CH profile is shown to illustrate the thin features of both the measured and computed CH* profiles.

Accurate computations of the CH, CH*, and OH* radicals pose a difficult numerical problem. For example, the concentration of CH can change by an order of magnitude within 0.1 mm. This requires that the adaptive grid be refined to an extremely small mesh size in the vicinity of high spatial activity.

Kinetics Modeling

To model chemiluminescence, the species CH* and OH* must be added to the kinetic mechanisms, along with a set of formation and destruction reactions with appropriate rate constants. All CH*/OH*-related rate constants used in this study are detailed in Table 1.

CH* is produced chemically via the reaction of the ethynyl radical with monatomic and diatomic oxygen:

$$\text{I)} \quad C_2H + O_2 \leftrightarrow CH^* + CO_2$$
$$\text{II)} \quad C_2H + O \leftrightarrow CH^* + CO$$

The rate constants have been reported as $k_I = 3.6 \times 10^{-14}$ cm^3 molecule^{-1} s^{-1} and $k_{II} = 1.8 \times 10^{-11}$ cm^3 molecule^{-1} s^{-1} [15]. The uncertainties associated with these reaction rates are about 40%. Destruction reactions occur by spontaneous emission ($CH^* \rightarrow CH + h\nu$) and collisional quenching. Quenching was modeled with seven different reactions, each involving CH* and a major chemical species in the flame (CH_4, N_2, O_2, H_2O, CO, CO_2, H_2). Species-specific, temperature-dependent quenching rates were taken from Tamura et al. [8]. The heat of formation of CH* was set at 66.3 kcal/mole above that of ground-state CH, based on the energy of the spontaneously emitted photon.

OH* formation was modeled with a single reaction:

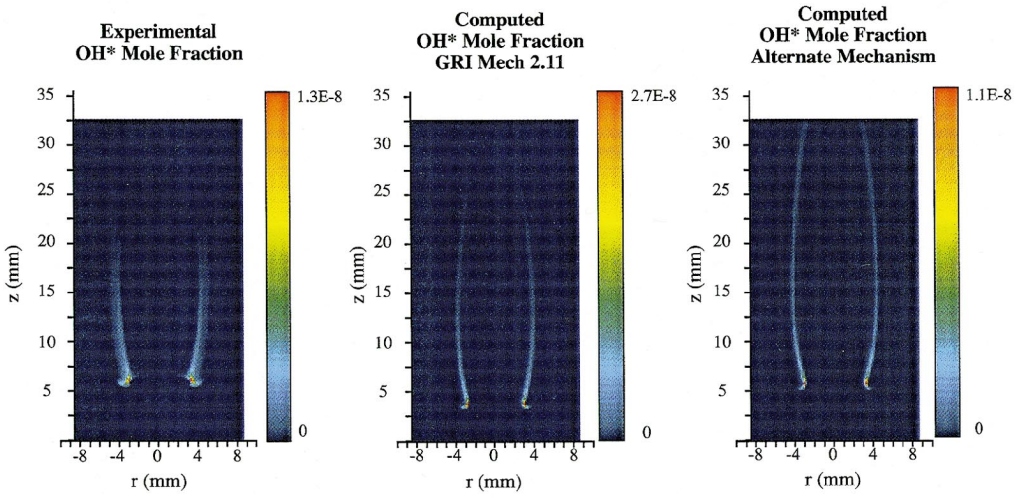

FIG. 3. OH* mole fraction profiles determined by measurement, GRI Mech 2.11, and an alternate hydrocarbon mechanism.

III) $CH + O_2 \leftrightarrow OH^* + CO$

The rate constant for the reaction $CH + O_2 \rightarrow$ All Products was measured by Berman [16]. This measurement was used for k_{III} by Marchese et al. [17] and will be used here as well. Uncertainty in this rate constant is likely to be large but is not readily estimated. Spontaneous emission and collisional quenching reactions were added to the mechanism in the same manner as previously described. The heat of formation of OH* was set at 93 kcal/mole above that of ground-state OH. Note that chemiexcitation reactions I–III all have other channels that form ground-state species, which are included in both kinetic schemes.

Results and Discussion

As with our previous investigations, GRI Mech 2.11 continues to produce very good agreement with the overall flame length observed in the experiments, while significantly underpredicting the flame lift-off height. The alternate kinetic scheme is much more accurate in predicting lift-off height but overpredicts the overall flame length. Note that the predicted lift-off height is related to the extinction strain rate obtained in the corresponding counterflow diffusion flame. The extinction strain rate computed with GRI Mech 2.11 is nearly 20% higher than that obtained with the alternate mechanism, and thus the flame can anchor itself in a region of higher strain.

The character of the CH distribution within the GRI-computed profile is in excellent agreement with the measurements; that is, the highest CH concentration appears near the flame anchoring region, falling off to a nearly constant level throughout the flame front, up to and including the tip of the flame front. The peak measured ground-state CH number density was 1.53×10^{13} cm^{-3}. Given that the temperature was measured in this flame previously, we can easily calculate mole fractions from measured concentrations. Hence, the measured peak mole fraction of CH is 4×10^{-6}, nearly 20% higher than the prediction of GRI Mech 2.11.

Other than a better prediction of the lift-off height, the computed CH results are not as good with the alternate hydrocarbon kinetic mechanism. The location and distribution of CH is still within reasonable agreement, but the CH profile no longer appears to close at the flame tip. Additionally, the peak CH concentration is predicted to be 42% lower than the measured concentration. The dependence of the spatial characteristics and absolute concentrations on the choice of kinetic scheme reveals CH to be an important test of our rather well-validated flame model, as subtle differences are not seen between the two kinetic schemes for the prediction of major species and temperature profiles.

The CH* profile is thinner than that of ground-state CH when comparing measured CH to measured CH*, as seen in Fig. 2. The difference in peak concentration of the experimental profiles of CH and CH* is of order 1000, similar to the ratio measured by other researchers [18]. A relationship similar to that discussed with CH exists between the computed profiles of CH* and the measurements, as far as spatial distribution and overall characteristics. However, the measured peak mole fraction of

TABLE 1
Reactions added for CH* and OH* kinetics. Units for rate constants are centimeters, moles, and seconds, with the formulation $k = AT^B \exp[-E_a/RT] - E_a$ in cal mole^{-1} and R in cal mole^{-1} K^{-1}

Reaction	A	B	E_a	Ref.
C2H + O = CH* + CO	1.08E + 13	0.00	0	[15]
C2H + O2 = CH* + CO2	2.17E + 10	0.00	0	[15]
CH* → CH	1.85E + 06	0.00	0	[8]
CH* + N2 = CH + N2	3.03E + 02	3.40	−381	[8]
CH* + O2 = CH + O2	2.48E + 06	2.14	−1720	[8]
CH* + H2O = CH + H2O	5.30E + 13	0.00	0	[8]
CH* + H2 = CH + H2	1.47E + 14	0.00	1361	[8]
CH* + CO2 = CH + CO2	2.40E − 01	4.30	−1694	[8]
CH* + CO = CH + CO	2.44E + 12	0.50	0	[8]
CH* + CH4 = CH + CH4	1.73E + 13	0.00	167	[8]
CH + O2 = OH* + CO	3.25E + 13	0.00	0	[16]
OH* → OH	1.45E + 06	0.00	0	[8]
OH* + N2 = OH + N2	1.08E + 11	0.50	−1238	[8]
OH* + O2 = OH + O2	2.10E + 12	0.50	−482	[8]
OH* + H2O = OH + H2O	5.92E + 12	0.50	−861	[8]
OH* + H2 = OH + H2	2.95E + 12	0.50	−444	[8]
OH* + CO2 = OH + CO2	2.75E + 12	0.50	−968	[8]
OH* + CO = OH + CO	3.23E + 12	0.50	−787	[8]
OH* + CH4 = OH + CH4	3.36E + 12	0.50	−635	[8]

CH*, 2×10^{-9}, is a factor of 17 and 33 greater than the predictions of the alternate mechanism and GRI Mech 2.11, respectively.

As with CH and CH*, the highest concentration of OH* is found at the anchoring region, as seen in Fig. 3. The measured OH* concentration profile appears somewhat broader than predicted by either set of kinetics, and the measured peak mole fraction is within 15% of the peak computed with the alternate mechanism.

Conclusions

In this study, we extended the results of previous combined numerical and experimental investigations of an axisymmetric laminar diffusion flame in which difference Raman spectroscopy, laser-induced fluorescence, and a multidimensional flame model were used to generate profiles of the temperature and major and minor species. We discussed issues related to the computation and measurement of CH, CH*, and OH* in an unconfined laminar flame in which a cylindrical fuel stream is surrounded by a coflowing oxidizer jet. Experimentally, CH radical concentrations were measured with laser-induced fluorescence, whereas CH* and OH* concentrations were measured with flame emission.

The results of this study indicate that GRI Mech 2.11 does an excellent job of predicting peak CH concentration, considering the ppm concentration levels and narrow spatial extent of the CH radical's profile, as well as the overall characteristics and shape of the CH profile. Other than a better prediction of flame lift-off height, the CH results are not nearly as good with our alternate hydrocarbon kinetic scheme.

As far as spatial distribution and overall characteristics are concerned, relationships similar to those observed between calculated and measured CH were observed for calculated and measured CH* and OH*, as well. Peak concentration levels for CH* were severely underpredicted with both kinetic schemes, while peak concentration levels of OH* agreed to within 15% (alternate mechanism) and a factor of 2 (GRI Mech 2.11) of the predicted peaks. Still, this indicates that although overall flame structure is well understood and well characterized, the formation and destruction kinetics associated with excited-state species in flames requires further research. The reasonable uncertainties in the excitation reaction rate constants for CH* production indicate it is likely that new formation pathways, such as $C_2 + OH \rightarrow CH^* + CO$ [11], need to be postulated and investigated.

Acknowledgments

We would like to thank Dr. J. H. Miller of George Washington University and Dr. J. B. Jeffries of SRI for helpful discussions. The support of NASA under Grant NAG3-1939 is gratefully acknowledged.

REFERENCES

1. Najm, H. N., Paul, P. H., Mueller, C. J., and Wyckoff, P. S., *Combust. Flame* 113:312–332 (1998).
2. Smooke, M. D., Lin, P., Lam, J., and Long, M. B., in *Twenty-Third Symposium (International) on Combustion,* The Combustion Institute, Pittsburgh, 1991, pp. 575–582.
3. Smooke, M. D., Xu, Y., Zurn, R. M., Lin, P., Frank, J. H., and Long, M. B., in *Twenty-Fourth Symposium (International) on Combustion,* The Combustion Institute, Pittsburgh, 1992, pp. 813–822.
4. Smooke, M. D., Ern, A., Tanoff, M. A., Valdati, B. A., Mohammed, R. K., Marran, D. F., and Long, M. B., in *Twenty-Sixth Symposium (International) on Combustion,* The Combustion Institute, Pittsburgh, 1996, pp. 2161–2170.
5. Marran, D. F., "Quantitative Two-Dimensional Laser Diagnostics in Idealized and Practical Combustion Systems," Ph. D. thesis, Yale University, New Haven, 1996.
6. Bonczyk, P. A. and Shirley, J. A., *Combust. Flame* 34:253–264 (1979).
7. Luque, J. and Crosley, D. R., *Appl. Phys. B* 63:91–98 (1996).
8. Tamura, M., Berg, P. A., Harrington, J. E., Luque, J., Jeffries, J. B., Smith, G. P., and Crosley, D. R., *Combust. Flame* 114(3-4):502–514 (1998).
9. Huber, K. P. and Herzberg, G., *Molecular Spectra and Molecular Structure IV. Constants of Diatomic Molecules,* Van Nostrand Reinhold Co., New York, 1979.
10. Luque, J. and Crosley, D. R., "LIFBase Database and Spectral Simulation Program (Version 1.0)," SRI International, Rept. MP 96-001 (1996).
11. Gaydon, A. G. and Wolfhard, H. G., *Flames,* Chapman and Hall, London, 1960.
12. Dasch, C. J., *Appl. Opt.,* 31:1146–1152 (1994).
13. Ern, A., Douglas, C. C., and Smooke, M. D., in *The International Journal of Supercomputer Applications,* vol. 9, no. 3, 1995, p. 167.
14. Bowman, C. T., Hanson, R. K., Davidson, D. F., Gardiner Jr., W. C., Lissianski, V., Smith, G. P., Golden, D. M., Frenklach, M., Wang, H., and Goldenberg, M., *GRI-Mech version 2.11,* http://www.gri.org, 1995.
15. Devriendt, K., Van Look, H., Ceursters, B., and Peeters, J., *Chem. Phys. Lett.* 261:450–456 (1996).
16. Berman, M. R., Fleming, J. W., Harvey, A. B., and Lin, M. C., in *Nineteenth Symposium (International) on Combustion,* The Combustion Institute, Pittsburgh, 1982, pp. 73–80.
17. Marchese, A. J., Dryer, F. L., Vedha-Nayagam, M., and Colantonio, R., in *Twenty-Sixth Symposium (International) on Combustion,* The Combustion Institute, Pittsburgh, 1996, pp. 1219–1226.
18. Joklik, R. G., Daily, J. W., and Pitz, W. J., in *Twenty-First Symposium (International) on Combustion,* The Combustion Institute, Pittsburgh, 1986, pp. 895–904.

COMMENTS

David R. Crosley, SRI International, USA. You predicted the CH concentration quite well, and of course you know O_2 even better. Thus, the correspondence between measured and predicted OH* depends only on a single rate coefficient and suggests some adjustment is needed. Does the predicted OH*, which differs between the two mechanisms, track directly the predicted CH?

Author's Reply. The peak mole fractions of both CH and OH* were greater using GRI Mech 2.11 than with the alternate mechanism (see table). However, if one forms the ratio of peak CH to peak OH* mole fractions using the two different mechanisms, the ratios differ by nearly a factor of 2. The location of the peak CH mole fraction in the GRI Mech calculation corresponds to a region with higher O_2 mole fraction compared to the calculation using the alternate mechanism. In regions where the CH exists, the CO mole fractions and temperatures are nearly the same for both calculations. As a result, when the effects of all four species are taken into account, the ratio $X_{CH}\ X_{O_2}/X_{OH^*}\ X_{CO}$ is essentially the same for the two mechanisms.

Peak Mole Fraction	GRI Mech 2.11	Alternate Mechanism
X_{CH}	3.30E-06	2.30E-06
X_{OH^*}	2.70E-08	1.10E-08

●

Steve Hasko, BG Technology plc, UK.

1. Did the authors use the same rate data in their alternate reaction scheme as they used in their implementation of GRI Mech? Otherwise, what was that scheme optimized against?
2. On the experimental and computed maps of temperature, the tip of the inner cone of the computed result seems to be sharper than that of the measured flame, which appears more rounded. It has been our experience that the strength of the tip can affect the lower edges and, thus, also the standoff height. Have the authors any thoughts about what might be happening at the tip, such as thermal diffusion of M atoms, that might cause this difference between the measured and computed results?

Author's Reply. The two mechanisms did not use the same rate data. The alternate mechanism was compared against experimental measurements for temperature and species in a variety of flame configurations (Ref. [3] in the paper and references therein).

The apparent sharpness at the tip of the inner cone seen in the computed temperature maps is due, in part, to the lower spatial resolution of the calculations at this downstream location. We note that the calculations using the two different mechanisms display a similar degree of sharpness, despite having quite different lift-off heights. Your observation is an interesting one, but we have not had an opportunity to investigate this further.

•

H. F. Calcote, ChemIon, Inc., USA. Ions in hydrocarbon–oxygen flames are due to the chemi-ionization reaction: CH + O → HCO + where the CH is usually considered to be the excited state CH($A^2\Delta$). Your work is thus of relevance toward quantitatively accounting for chemi-ions. The rate coefficient for the foregoing reaction with CH($A^2\Delta$) has been reported as 4.8E + 14 [1] as measured in a flame by Cool and Tjossem [2]. How would the inclusion of this reaction in Table 1 affect your results?

Table 1 includes three reactions with negative activation energies. Could you comment on these reactions in terms of Benson and Dobis recent discussion [3] of negative activation energy reactions? They argue that such reactions are an artifact of the experiment or they are due to a multistep transition-state mechanism.

REFERENCES

1. Filakov, A. B., *Prog. Energy Combust. Sci.* 23:399–528 (1997).
2. Cool, T. A. and Tjossem, P. J. H., *Chem. Phys. Lett.* 111:82–88 (1984).
3. Benson, S. W. and Dobis, O., *J. Phys. Chem. A* 102:5175–5181 (1998).

Author's Reply. The rate constant for the chemi-ionization step is approximately a factor of 4 (for CO and H_2) to an order of magnitude (for O_2, N_2, and CO_2) higher than the rate constants we used in our CH* collisional deactivation steps in the region of the flame where CH* is present. However, considering the magnitude of the O-atom concentration compared with the concentration of the collisional partners in this region (e.g., N_2), the chemi-ionization step will have little impact on the consumption of CH*.

Benson and Dobis discuss the apparent nature of negative activation energies for certain bimolecular metathesis reactions. However, the negative activation energies quoted for three of the CH* collisional deactivation steps (as well as the OH* collisional deactivation steps) are neither an experimental artifact nor due to a multistep transition-state mechanism. The three parameter pseudo-Arrhenius forms used by Tamura et al. (our Ref. [8]), are taken from the compilation of Heinrich and Stuhl [1], who determined best fits of their experimentally determined quenching rate constants grouped with a variety of previously quoted literature values in alternate temperature ranges. Indeed, Heinrich and Stuhl noted the difficulty in fitting the observed temperature dependencies with physically meaningful rate parameters. While the sum of two Arrhenius forms was observed to be a good representation of the date, the authors found no indication that the quenching reactions occurred via two paths with distinct activation energies and thus opted for the more general three-parameter pseudo-Arrhenius form.

REFERENCE

1. Heinrich, P. and Stuhl, F., *Chem. Phys.* 199:105–118 (1995).